Dalton Transactions

ROYAL SOCIETY OF CHEMISTRY

PAPER

View Article Online
View Journal | View Issue

Cite this: *Dalton Trans.*, 2025, **54**, 1618

Fine-tuning of optical band gap in mixed halide aziridinium lead perovskites†

Olesia I. Kucheriv, ‡[a] Dmytro A. Haleliuk,‡[a] Sergiu Shova[b] and Il'ya A. Gural'skiy *[a]

Received 14th October 2024,
Accepted 27th November 2024

DOI: 10.1039/d4dt02879a

rsc.li/dalton

Hybrid halide perovskites form a promising class of light-absorbing materials. Among the numerous 3D semiconducting perovskites, there is a group of emerging aziridinium-based hybrids that are considered to be prospective materials for optoelectronic applications. In this work, we report the mixed halide aziridinium perovskites of **(AzrH)PbBr$_x$I$_{3-x}$** series (AzrH = aziridinium). Small changes in the composition of perovskites are shown to have a defining impact on the optoelectronic properties of the reported materials. Halogen substitution allowed a variation in band gap values of these compounds, ranging from 1.57 to 2.23 eV, as established using electronic spectroscopy. Crystal structures of **(AzrH)PbBr$_x$I$_{3-x}$** perovskites were studied using single crystal and powder X-ray diffraction analysis. The lattice constant had a linear dependence on the Br content in the structure, thus strictly following Vegards's law. Importantly, the reported compounds displayed a preferential inclusion of iodine upon synthesis, revealing that the mixed halide perovskite composition cannot be estimated based on the precursors' ratio only, and it should be post-synthetically checked. The reported results expand the range of hybrid perovskites with tuneable band gaps beyond the conventional methylammonium and formamidinium-based perovskites and offer a new series of metal-halide hybrids suitable for photovoltaic and other optoelectronic applications.

Introduction

Hybrid halide perovskites attract significant attention as photoabsorbers in various optoelectronic applications.[1–3] The materials themselves were first reported in 1978 by Weber *et al.*[4,5] However, the rapid developments in perovskite research started only in 2009 when Kojima *et al.* demonstrated the potential applications of hybrid perovskite in photovoltaic devices.[6] Even though the efficiency of the first prototypes was quite low and they had some stability issues, the significant effort that has been put into the development of this research field allowed obtaining perovskite solar cells with efficiency exceeding 25%.[7] Such increasing values of efficiency and inexpensive precursors, along with simple solution-based deposition approaches, make hybrid perovskites highly attractive materials for the rapidly growing industry of solar cell technology.[8] In addition, hybrid perovskites have also been successfully implemented as active layers in light emitting diodes,[9] lasers,[10] thermoelectric couplers,[11] used for water splitting applications,[12] photodetection[13] and more.

Hybrid halide perovskites have a general formula ABX_3, where A is an organic cation, B is a cation of divalent metal (usually Pb^{2+} or Sn^{2+}), and X is a halogen anion (Cl^-, Br^- or I^-). In its crystal structure, the hybrid perovskite is composed of $[BX_6]$ octahedra that are assembled in a corner-sharing manner into an infinite 3D framework. Among these octahedra there are cuboctahedral voids that are occupied by organic cations. Limited space in the framework voids sets very strict geometrical limitations on the size of the organic cation. A cation that is too big for the void will induce the formation of layered low-dimensional perovskites, while a cation that is too small will cause an excessive strain, preventing the formation of the framework. The most commonly studied and used hybrid perovskites are based on methylammonium (MA). $MAPbI_3$ is considered to be a background standard material that is used for all the subsequent modifications.[14] This cation is quite often replaced with formamidinium (FA), which also has high efficiency for photovoltaic applications.[15–19] Simultaneously, in recent years, several new organic cations, such as aziridinium,[20–23] methylhydrazinium[24–27] and a few others,[28–30] have been found to be suitable for the formation of 3D hybrid perovskite structures.

[a]*Department of Chemistry, Taras Shevchenko National University of Kyiv, Volodymyrska St. 64, 01601 Kyiv, Ukraine. E-mail: illia.guralskyi@univ.kiev.ua*
[b]*Department of Inorganic Polymers, "Petru Poni" Institute of Macromolecular Chemistry, 41A Aleea Gr. Ghica Voda, 700487 Iasi, Romania*

†Electronic supplementary information (ESI) available: Crystallographic tables, Goldschmidt's tolerance factors. CCDC 2390779–2390785. For ESI and crystallographic data in CIF or other electronic format see DOI: https://doi.org/10.1039/d4dt02879a

‡These authors contributed equally to this work.

An important feature of the hybrid halide perovskites that makes them beneficial, in comparison with commercially used semiconductors, is the simplicity of their synthesis through widespread solution-based approaches. These approaches allow very simple, yet elegant, engineering of the chemical composition of the hybrid perovskites, which has a significant impact on their photophysical properties. In particular, the composition allows modification of the band gap of these materials. Modification of the A-site cation (for example, partial substitution of MA with FA) usually enables quite minor changes in the band gap values in the order of 0.1 eV.[14] Simultaneously, the substitution of I with Br has been shown to allow band gap modification from 1.5 eV (for pure I perovskites) to *ca.* 2.3 eV (for pure Br perovskites). Such a substitution has been studied for both MA[31–33] and FA[34] perovskites. Supposedly, the same substitution is possible for the I and Cl combination, it could allow a band gap tuning in an even larger range. However, in practice, there are certain obstacles that emerge upon the introduction of chloride,[35] making the Br/I system the most promising for further investigations.

In this paper, we report a series of new semiconducting materials for optoelectronic applications: mixed **(AzrH)PbBr$_x$I$_{3-x}$** perovskites in both single crystal and polycrystalline form, as well as their structural and spectroscopic characterization.

Results and discussion

The crystal structures of aziridinium lead mixed halide perovskites were studied by performing seven SXRD measurements on crystals with different Br/I ratios (Tables 1 and S2.1–S8.3†). All obtained materials crystalize in cubic $Pm\bar{3}m$ space group, same as (AzrH)PbBr$_3$ and (AzrH)PbI$_3$ perovskites. In their crystal structure, the [PbX$_6$] octahedra are connected with each other in an infinite 3D framework in a corner-sharing manner (Fig. 1). Voids between the inorganic octahedra are filled with organic aziridinium cations that are disordered among multiple positions at the temperatures of the experiments. It is worth noting that the offered solutions for aziridinium disorder are only a couple of multiple possible ways to model this cation. Aziridinium cation interacts with the inorganic framework *via* N–H···Hal hydrogen bonds.

Single crystal XRD experiments are a precise tool for determining unit cell parameters for all perovskites in the obtained series and to refine the ratio of Br and I as these halogens have considerably different contributions to the electronic density in the structure. The plot of cell parameter a as a function of Br content x is given in Fig. 2. The obtained plot has a linear dependence that can be linearized by the following function:

$$a = 6.3577 - 1.2996x_{\mathrm{Br}}. \quad (1)$$

A linear descent of the given dependance with x_{Br} growth is observed in **(AzrH)PbBr$_x$I$_{3-x}$** mixed halide perovskites, following the empirical Vegard's law. This suggests that these materials form random solid solutions. A similar linear trend of cell parameter dependance has been observed for MAPbBr$_x$I$_{3-x}$ solid solutions for the x_{Br} = 0.24–2.73 range, in which the formation of the cubic form is supported.[36] Meanwhile, iodine-rich samples of MAPbBr$_x$I$_{3-x}$ tend to form a tetragonal phase.

According to Goldschmidt's rule, the formation of a perovskite 3D structure is possible, when the tolerance factor t lies in the range of 0.8–1:

$$t = \frac{r_{\mathrm{Aeff}} + r_{\mathrm{Xeff}}}{\sqrt{2}(r_{\mathrm{Beff}} + r_{\mathrm{Xeff}})}, \quad 0.8 \le t \le 1, \quad (2)$$

where r_{Aeff} is the effective radius of the organic cation; r_{Beff} is the effective radius of B-site cation, and r_{Xeff} is the effective radius of the halogen.

The value of the tolerance factor is 0.956 for (AzrH)PbBr$_3$ and 0.939 for (AzrH)PbI$_3$. As the Pb–X bond lengths follow Vegard's rule in the **(AzrH)PbBr$_x$I$_{3-x}$** series, the tolerance factor in these mixed halide perovskites also drops linearly with the decrease in the Br content (Table S1†). It is worth noting that the Pb–Hal bond length obtained from the SXRD experiments is always lower than the sum of calculated effective ionic radii (by 0.163 Å for (AzrH)PbBr$_3$ and by 0.208 Å for (AzrH)PbI$_3$), indicating the partially covalent nature of the Pb–Hal bonds in the hybrid perovskites.

Table 1 Crystallographic parameters of the **(AzrH)PbBr$_x$I$_{3-x}$** series

	(AzrH)PbBr$_{0.04}$I$_{2.96}$	**(AzrH)PbBr$_{0.09}$I$_{2.91}$**	**(AzrH)PbBr$_{0.85}$I$_{2.15}$**	**(AzrH)PbBr$_{1.96}$I$_{1.04}$**	**(AzrH)PbBr$_{2.01}$I$_{0.99}$**	**(AzrH)PbBr$_{2.08}$I$_{0.92}$**	**(AzrH)PbBr$_{2.79}$I$_{0.21}$**
Temperature (K)	250	250	293	230	293	250	293
Crystal system	Cubic	Cubic	Cubic	Cubic	Cubic	Cubic	Cubic
Space group	$Pm\bar{3}m$	$Pm\bar{3}m$	$Pm\bar{3}m$	$Pm\bar{3}m$	$Pm\bar{3}m$	$Pm\bar{3}m$	$Pm\bar{3}m$
a (Å)	6.35060(10)	6.33861(18)	6.2570(2)	6.10960(10)	6.0891(2)	6.0775(3)	5.9968(3)
Volume (Å^3)	256.120(12)	254.67(2)	244.96(2)	228.054(11)	225.77(2)	224.48(3)	215.65(3)
Z	1	1	1	1	1	1	1
$\rho_{\mathrm{calc.}}$ (g cm^{-3})	4.046	4.054	3.972	3.887	3.909	3.907	3.806
Goodness-of-fit on F^2	1.132	1.250	1.185	1.227	1.001	1.116	1.174
R_1 [$I > 2\sigma(I)$]	0.0300	0.0140	0.0663	0.0171	0.0353	0.0176	0.0437
wR_2 [all data]	0.0861	0.0428	0.1852	0.0578	0.0847	0.0423	0.1073

$R_1 = \sum||F_o| - |F_c||/\sum|F_o|$ and $wR_2 = [\sum w(F_o^2 - F_c^2)^2/\sum w(F_o^2)^2]^{1/2}$ for $F_o^2 > 2\sigma(F_o^2)$.

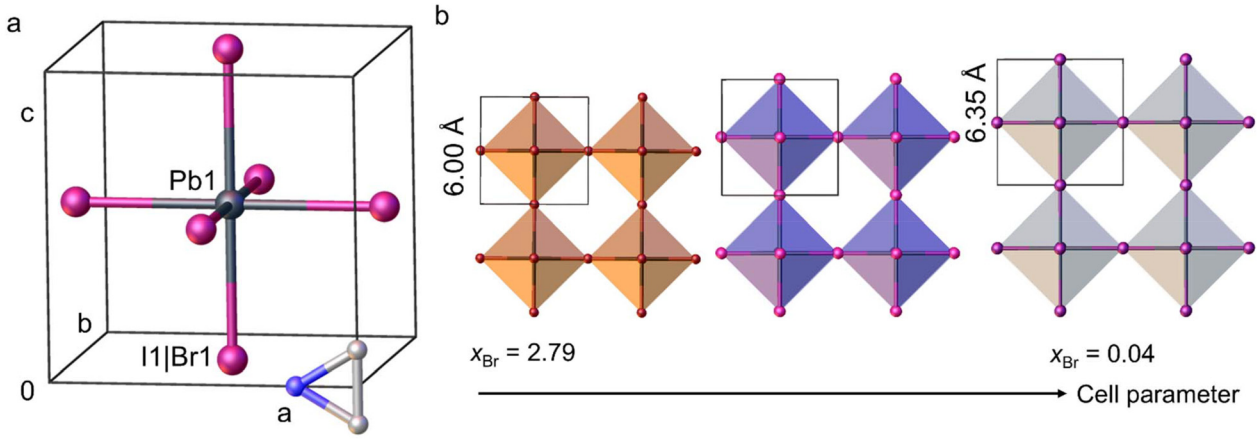

Fig. 1 (a) Unit cell of aziridinium mixed halide perovskites showing $[PbBr_{2x}I_{6-2x}]$ octahedron and aziridinium cation. The crystal structure of (**AzrH**)**PbBr$_{2.01}$I$_{0.99}$** was used to draw the image. Aziridinium disorder is not shown for clarity. (b) Selected fragments of **(AzrH)PbBr$_x$I$_{3-x}$** frameworks demonstrate the increase in cell parameters upon variation in the Br/I ratio.

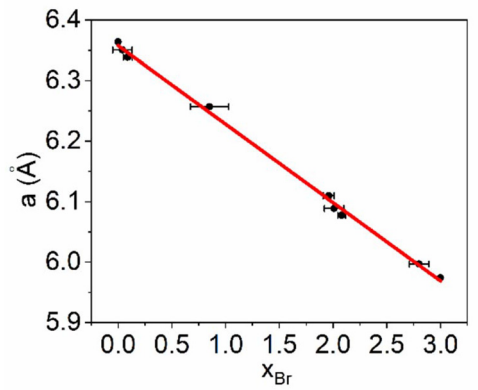

Fig. 2 Dependance of the cell parameter *a* on the x_{Br} content in mixed halide **(AzrH)PbBr$_x$I$_{3-x}$** perovskites.

In addition, a series of polycrystalline **(AzrH)PbBr$_x$I$_{3-x}$** mixed halide perovskite samples were obtained in bulk form. The phase purity of the polycrystalline samples was established using PXRD measurements (Fig. 3). Experimental PXRD patterns are in good agreement with patterns calculated from the SXRD data, confirming the formation of a pure cubic $Pm\bar{3}m$ phase for all the obtained materials. Upon increase in the Br content (*i.e.*, x) in the obtained materials, 2θ values of some characteristic peaks shift from 27.97° (002), 31.36° (012), 40.11° (022), and 42.42° (003) for x_{Br} = 0.00 to 29.78° (002), 33.41° (012), 42.60° (022) and 45.24° (003) for x_{Br} = 2.73. In addition, the peak at 24.13°, corresponding to the (111) plane for x_{Br} = 0.00, almost disappears for x_{Br} = 2.73.

The direct refinement of the halogen ratio from PXRD peak intensity is not very precise, as the intensity of peaks is usually strongly affected by preferential orientation and other factors. Meanwhile, indexing of the PXRD patterns provides precise values of unit cell parameters, especially in the case of the title perovskite materials with cubic structures. This is the reason

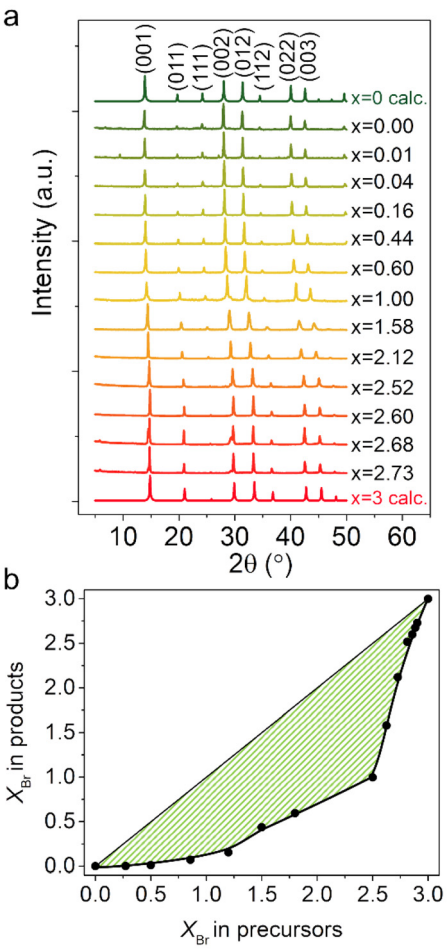

Fig. 3 (a) Experimental PXRD patterns of polycrystalline **(AzrH)PbBr$_x$I$_{3-x}$** mixed halide perovskite samples, in comparison with the calculated patterns for (AzrH)PbI$_3$ and (AzrH)PbBr$_3$.[23] The mentioned Br content x is determined from cell lattice parameters. (b) The dependance of x_{Br} in the obtained products on the x_{Br} in the precursor solutions shows a significant preferential inclusion of iodine. A line is drawn to guide the eye.

why we used unit cell parameters to extract the halogen ratio by means of dependance as shown in Fig. 2.

Indexing of patterns and comparison of obtained cell parameters revealed a notable difference in the Br/I ratio in the precursor solutions and in the resulting mixed halide perovskites (Fig. 3b). In the case of **(AzrH)PbBr$_x$I$_{3-x}$** series, a significant preferential inclusion of iodine is observed. From the chemical point of view, this effect can be explained in line with hard and soft acids and bases theory, according to which the iodine anion is a soft Lewis base, while the bromine anion is a relatively harder base. Considering that the lead cation is a soft Lewis acid,[37] creating a bond with iodine is more energetically beneficial for it. In addition, this observation makes an important demonstration of the fact that estimation of mixed halide composition from the precursors' ratio is not always possible.

The optical properties of polycrystalline **(AzrH)PbBr$_x$I$_{3-x}$** mixed halide perovskite samples were studied by measuring their optical reflectance spectra (Fig. 4). All materials displayed a characteristic cut-off of reflectance, which is typical for semiconducting materials. The cut-off wavelength shifted gradually from 794 nm for x = 0.07 to 550 nm for x = 2.68, thus covering a yellow-to-red range of visible spectrum and even partially covering the near-IR range. Optical photographs of selected powder samples are given in Fig. 4b that show a change in the samples' color upon halogen substitution from orange to black.

Optical band gap values can be extracted from the experimentally determined absorption coefficient using a Tauc plot based on the equation:

$$(\alpha h\upsilon)^{1/n} = A(h\upsilon - E_g), \quad (3)$$

where α is an absorption coefficient; h is the Plank constant; υ is a frequency; E_g is an optical band gap; A is a proportionality constant that depends on transition probability, and n is a Tauc coefficient which is determined by the type of transition. This is true for cases of direct band gap semiconductors with allowed transitions, for which $n = \frac{1}{2}$.

When reflectance spectra are obtained experimentally, instead of the absorbance spectra, the Kubelka–Munk function has to be applied. According to this:

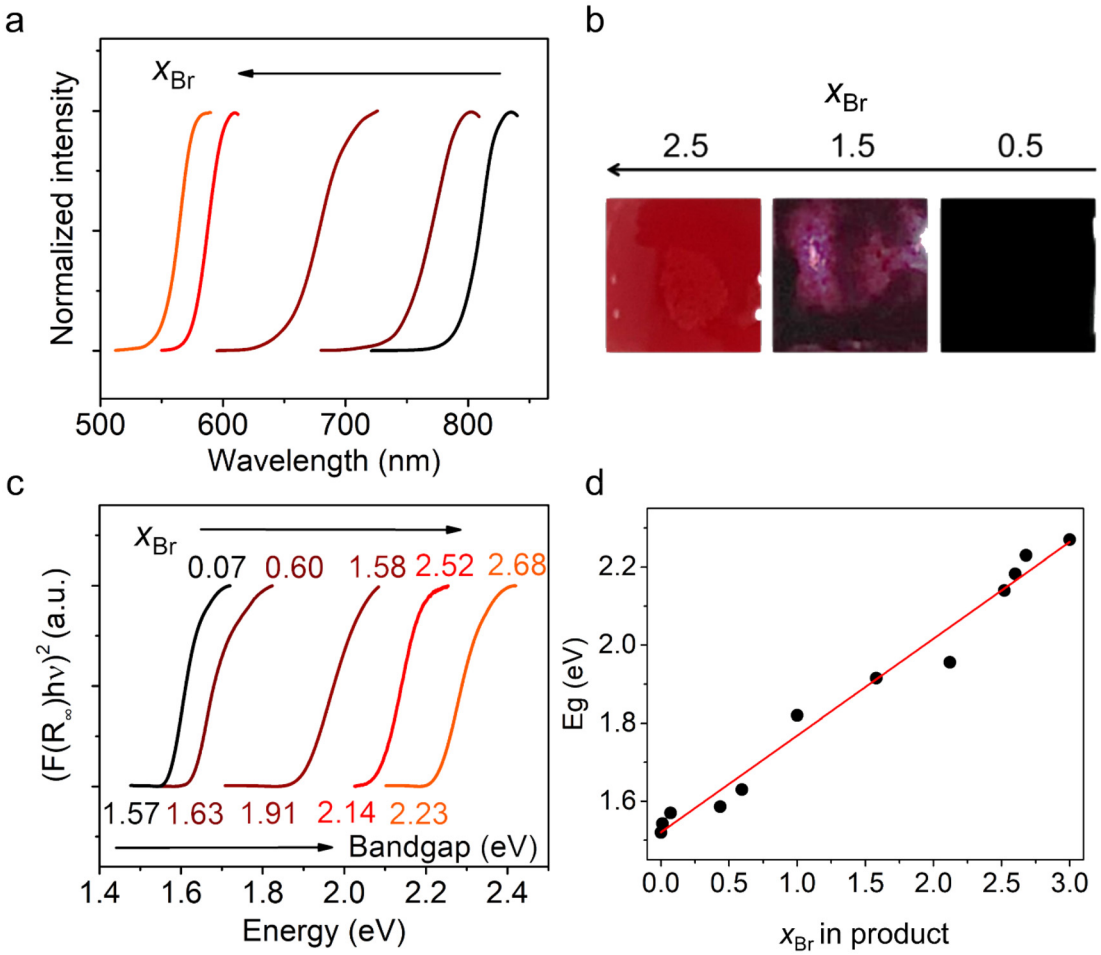

Fig. 4 (a) Optical reflectance spectra of polycrystalline **(AzrH)PbBr$_x$I$_{3-x}$** mixed halide perovskite samples. (b) Photographs of selected **(AzrH)PbBr$_x$I$_{3-x}$** powder samples showing color change upon halogen substitution. (c) Kubelka–Munk plots of polycrystalline **(AzrH)PbBr$_x$I$_{3-x}$** perovskite samples show a gradual shift in the band gap upon halogen substitution. (d) Demonstration of a linear trend in E_g *vs.* x_{Br} dependance.

$$F(R) = \frac{\alpha}{S} = \frac{(1 - R_\infty)^2}{2R_\infty}. \quad (4)$$

The function $F(R)$ is directly proportional to the absorption coefficient α and inversely proportional to the scattering S, while R_∞ is the diffuse reflectance of the sample. Thus, the optical band gap of the studied materials value can be extracted by plotting the following function:

$$(h\upsilon F(R_\infty))^2 = A(h\upsilon - E_g). \quad (5)$$

The Tauc plots for polycrystalline **(AzrH)PbBr$_x$I$_{3-x}$** mixed halide perovskite samples are shown in Fig. 4c. The band gap of the studied materials varies in the range of 1.57 eV (for x_{Br} = 0.07) − 2.23 eV (for x_{Br} = 2.68). The conservation of a cubic structure for the whole series of **(AzrH)PbBr$_x$I$_{3-x}$** solid solutions is important and a linear dependance of the cell parameter on the Br content causes a linear dependance of band gap on the Br content (Fig. 4d). This dependance can be linearized as follows:

$$E_g = 1.520 + 0.248x_{Br}. \quad (6)$$

This linear dependance provides additional proof that the materials from the studied series are semiconductors that follow Vegard's law.

For comparison, the E_g dependance on the cell parameter in MAPbBr$_x$I$_{3-x}$ series (x_{Br} = 0.24–2.73) has been shown to obey the dependency described by a quadratic equation. Simultaneously, the iodine-rich samples tend to display significant deviation from this dependence, which can be explained by the formation of a tetragonal phase for this composition.[36]

Notably, these samples do not have any considerable fluorescence at room temperature. However, the title Br perovskite is known to have fluorescence at low temperatures or when processed to NPs (sometimes referred to as perovskite quantum dots). Therefore, the linear dependance of band gap on x_{Br} content in **(AzrH)PbBr$_x$I$_{3-x}$** series has a significant advantage for further application in optoelectronic devices, such as light emitting diodes, due to the possibility of conducting more straightforward prediction of photoluminescence wavelength upon fabrication of devices.

Experimental

Chemicals and reagents

Aziridine, lead bromide, lead iodide, hydrobromic (48%), and hydroiodic acids (57%) were purchased from UkrOrgSyntez Ltd.

Synthetic procedures

(AzrH)PbBr$_x$I$_{3-x}$ powder samples. Lead bromide and iodide in selected ratios were dissolved in HBr/HI mixtures and diluted with distilled water (the exact quantities are given in Table 2).

6 eq. of aziridine were dissolved in a water/acetonitrile mixture. Afterward, the latter solution was added portion-wise to the lead halide solution with constant stirring.

(AzrH)PbBr$_x$I$_{3-x}$ single crystals. Lead bromide and iodide in selected ratios were dissolved in HBr/HI mixtures and diluted with distilled water (Table 2). The obtained solution was placed in a 1 mL vial, which was then placed in a bigger vial with 6 eq. of aziridine in water/acetonitrile mixture. After the diffusion of aziridine vapors small crystals were formed on the surface of lead halide solution and were separated after 1.5 h. The crystals were kept in a crystallographic oil until measurements were performed.

Measurements and characterization

Single-crystal X-ray diffraction. Single-crystal X-ray diffraction data were collected on Rigaku XtaLAB Synergy Dualflex HyPix diffractometer with graphite-monochromated Mo-Kα or Cu-Kα radiation or Oxford-diffraction XCALIBUR Eos CCD diffractometer with graphite-monochromated Mo-Kα radiation. The

Table 2 Quantitates of precursors used for the synthesis of **(AzrH)PbBr$_x$I$_{3-x}$** mixed halide perovskites powder samples

			PbI_2		$PbBr_2$		HI	HBr	H_2O	Azr	MeCN	H_2O
Br : I ratio	x_{Br} in precursors	x_{Br} in products[a]	mmol	mg	mmol	mg	mL	mL	mL	μL	mL	mL
30 : 1	2.90	2.73	0.0065	3.00	0.1951	71.60	0.02	0.60	1.00	63.00	0.10	0.20
25 : 1	2.88	2.68	0.0065	3.00	0.1627	59.70	0.03	0.60	1.00	53.00	0.10	0.20
20 : 1	2.86	2.60	0.0108	5.00	0.2169	79.60	0.04	0.60	1.00	71.00	0.10	0.20
15 : 1	2.81	2.52	0.0108	5.00	0.1627	59.70	0.05	0.60	1.00	54.00	0.20	0.20
10 : 1	2.73	2.12	0.0108	5.00	0.1084	39.80	0.05	0.40	0.80	37.00	0.20	0.20
7 : 1	2.63	1.58	0.0325	15.00	0.2278	83.60	0.10	0.60	0.80	82.00	0.50	0.20
5 : 1	2.50	1.00	0.0217	10.00	0.1084	39.80	0.10	0.40	0.80	41.00	0.50	0.20
1.5 : 1	1.80	0.60	0.0868	40.00	0.1302	47.80	0.40	0.50	0.80	68.00	0.50	0.20
1 : 1	1.50	0.44	0.0868	40.00	0.0872	32.00	0.24	0.20	0.80	54.00	0.80	0.20
1 : 1.5	1.20	0.16	0.1226	56.50	0.0817	30.00	0.30	0.17	0.50	64.00	0.80	0.20
1 : 2.5	0.86	0.07	0.1022	47.10	0.0409	15.00	0.40	0.13	0.50	45.00	1.00	0.20
1 : 5	0.50	0.01	0.1362	62.80	0.0272	10.00	0.40	0.07	0.50	31.00	1.00	0.20
1 : 10	0.27	0.00	0.1356	62.50	0.0136	5.00	0.30	0.03	0.50	47.00	1.00	0.20

[a] x_{Br} in products established by indexing their PXRD patterns and comparing the cell parameters obtained with results derived from the SXRD measurements.

unit cell determination and data integration were carried out using the CrysAlisPro package from Oxford diffraction. The structures were solved with the ShelXT program using the intrinsic phasing method and refined using the full-matrix least-squares method on F^2 with ShelXL.[38,39] Olex^2 was used as an interface for the ShelX programs.[40] Lead and halogen atoms were refined anisotropically in all structures. C and N atoms of disordered aziridinium cations were refined isotropically in most of the structures. The crystallographic data of the structures described in this paper were deposited at the Cambridge Crystallographic Data Center (CCDC 2390779–2390785†).

Optical reflectance measurements were performed on a Shimadzu spectrometer RF6000.

The PXRD patterns were acquired on a Shimadzu XRD-6000 diffractometer using Cu-Kα radiation (5–50°, 0.05° step) and Benchtop Rigaku Miniflex 600 diffractometer using Cu-Kα radiation (2–50°, 0.025° step).

Conclusions

In this work, we describe a new series of mixed halide lead perovskites with an aziridinium cation. Each of the reported materials contains a single crystalline phase which has a three-dimensional cubic structure. The cell parameters display a linear decrease with a decrease in the bromide content, proving that the reported materials obey the empirical Vegard's law and form solid solutions. It was established that iodine has significant preferential inclusion into the framework upon synthesis. Importantly, the variation in halogen content allows for fine-tuning of the absorption edge of aziridinium lead perovskite: a decrease in the bromide content leads to a linear red shift of the absorption cut-off. The optical band gap can be tuned in the 1.57–2.23 eV range. This effect makes the mixed halide aziridinium perovskites appealing candidates for further optoelectronic applications.

Author contributions

Olesia I. Kucheriv – writing – original draft, formal analysis; Dmytro A. Haleliuk – investigation, formal analysis; Sergiu Shova – investigation, formal analysis; Il'ya A. Gural'skiy – supervision, conceptualization, funding acquisition, writing – review & editing.

Data availability

Crystallographic data for **(AzrH)PbBr$_{0.04}$I$_{2.96}$**, **(AzrH)PbBr$_{0.09}$I$_{2.91}$**, **(AzrH)PbBr$_{0.85}$I$_{2.15}$**, **(AzrH)PbBr$_{1.96}$I$_{1.04}$**, **(AzrH)PbBr$_{2.01}$I$_{0.99}$**, **(AzrH)PbBr$_{2.08}$I$_{0.92}$**, and **(AzrH)PbBr$_{2.79}$I$_{0.21}$** were deposited at Cambridge Crystallographic Data Center under CCDC numbers 2390779–2390785† and can be obtained from **https://www.ccdc.cam.ac.uk/**.

Conflicts of interest

There are no conflicts to declare.

Acknowledgements

The authors acknowledge the financial support from the Ministry of Education and Science of Ukraine (grant no 24BF037-02 and grant no 24DF037-03H financed by the external aid instrument of the European Union to fulfill the obligations of Ukraine in the European Union Framework Program for Scientific Research and Innovation "Horizon 2020"). The authors also acknowledge the courage of the Armed Forces of Ukraine that made the submission of this manuscript possible.

References

1 Y. Zhao and K. Zhu, *Chem. Soc. Rev.*, 2016, **45**, 655–689.
2 W. Li, Z. Wang, F. Deschler, S. Gao, R. H. Friend and A. K. Cheetham, *Nat. Rev. Mater.*, 2017, **2**, 16099.
3 A. Younis, C. Lin, X. Guan, S. Shahrokhi, C. Huang, Y. Wang, T. He, S. Singh, L. Hu, J. R. D. Retamal, J. He and T. Wu, *Adv. Mater.*, 2021, **33**, 2005000.
4 D. Weber, *Z. Naturforsch., B*, 1978, **33**, 862–865.
5 D. Weber, *Z. Naturforsch., B*, 1978, **33**, 1443–1445.
6 A. Kojima, K. Teshima, Y. Shirai and T. Miyasaka, *J. Am. Chem. Soc.*, 2009, **131**, 6050–6051.
7 M. Kim, J. Jeong, H. Lu, T. K. Lee, F. T. Eickemeyer, Y. Liu, I. W. Choi, S. J. Choi, Y. Jo, H.-B. Kim, S. Mo, Y.-K. Kim, H. Lee, N. G. An, S. Cho, W. R. Tress, S. M. Zakeeruddin, A. Hagfeldt, J. Y. Kim, M. Grätzel and D. S. Kim, *Science*, 2022, **375**, 302–306.
8 B. Niu, H. Liu, Y. Huang, E. Gu, M. Yan, Z. Shen, K. Yan, B. Yan, J. Yao, Y. Fang, H. Chen and C. Li, *Adv. Mater.*, 2023, **35**, 2212258.
9 S. Ju, Y. Zhu, H. Hu, Y. Liu, Z. Xu, J. Zheng, C. Mao, Y. Yu, K. Yang, L. Lin, T. Guo and F. Li, *Light: Sci. Appl.*, 2022, **11**, 331.
10 Y.-J. Lu, T. L. Shen, K. Peng, P. Cheng, S. Chang, M. Lu, C. W. Chu, T. Guo and H. A. Atwater, *ACS Photonics*, 2021, **8**, 335–342.
11 W. Tang, J. Zhang, S. Ratnasingham, F. Liscio, K. Chen, T. Liu, K. Wan, E. S. Galindez, E. Bilotti, M. Reece, M. Baxendale, S. Milita, M. A. McLachlan, L. Su and O. Fenwick, *J. Mater. Chem. A*, 2020, **8**, 13594–13599.
12 H. Park, I. J. Park, M. G. Lee, K. C. Kwon, S. Hong, D. H. Kim, S. A. Lee, T. H. Lee, C. Kim, C. W. Moon, D. Son, G. H. Jung, H. S. Yang, J. R. Lee, J. Lee, N. Park, S. Y. Kim, J. Y. Kim and H. W. Jang, *ACS Appl. Mater. Interfaces*, 2019, **11**, 33835–33843.
13 N. R. Al Amin, C.-C. Lee, Y.-C. Huang, C.-J. Shih, R. Estrada, S. Biring, M.-H. Kuo, C.-F. Li, Y.-C. Huang and

S.-W. Liu, *ACS Appl. Mater. Interfaces*, 2023, **15**, 21284–21295.
14 T. J. Jacobsson, J.-P. Correa-Baena, M. Pazoki, M. Saliba, K. Schenk, M. Grätzel and A. Hagfeldt, *Energy Environ. Sci.*, 2016, **9**, 1706–1724.
15 Y. Zhang, Y. Li, L. Zhang, H. Hu, Z. Tang, B. Xu and N. Park, *Adv. Energy Mater.*, 2021, **11**, 2102538.
16 J. Jeong, M. Kim, J. Seo, H. Lu, P. Ahlawat, A. Mishra, Y. Yang, M. A. Hope, F. T. Eickemeyer, M. Kim, Y. J. Yoon, I. W. Choi, B. P. Darwich, S. J. Choi, Y. Jo, J. H. Lee, B. Walker, S. M. Zakeeruddin, L. Emsley, U. Rothlisberger, A. Hagfeldt, D. S. Kim, M. Grätzel and J. Y. Kim, *Nature*, 2021, **592**, 381–385.
17 Z. Xiong, L. Lan, Y. Wang, C. Lu, S. Qin, S. Chen, L. Zhou, C. Zhu, S. Li, L. Meng, K. Sun and Y. Li, *ACS Energy Lett.*, 2021, **6**, 3824–3830.
18 Z. Qin, Y. Chen, X. Wang, N. Wei, X. Liu, H. Chen, Y. Miao and Y. Zhao, *Adv. Mater.*, 2022, **34**, 2203143.
19 Z. Huang, Y. Bai, X. Huang, J. Li, Y. Wu, Y. Chen, K. Li, X. Niu, N. Li, G. Liu, Y. Zhang, H. Zai, Q. Chen, T. Lei, L. Wang and H. Zhou, *Nature*, 2023, **623**, 531–537.
20 O. I. Kucheriv, V. Y. Sirenko, H. R. Petrosova, V. A. Pavlenko, S. Shova and I. A. Gural'skiy, *Inorg. Chem. Front.*, 2023, **10**, 6953–6963.
21 O. A. Semenikhin, O. I. Kucheriv, L. Sacarescu, S. Shova and I. A. Gural'skiy, *Chem. Commun.*, 2023, **59**, 3566–3569.
22 M. Mączka, M. Ptak, A. Gągor, J. K. Zaręba, X. Liang, S. Balčiūnas, O. A. Semenikhin, O. I. Kucheriv, I. A. Gural'skiy, S. Shova, A. Walsh, J. Banys and M. Šimėnas, *Chem. Mater.*, 2023, **35**, 9725–9738.
23 H. R. Petrosova, O. I. Kucheriv, S. Shova and I. A. Gural'skiy, *Chem. Commun.*, 2022, **58**, 5745–5748.
24 D. Drozdowski, A. Gągor, D. Stefańska, J. K. Zareba, K. Fedoruk, M. Mączka and A. Sieradzki, *J. Phys. Chem. C*, 2022, **126**, 1600–1610.
25 M. Mączka, M. Ptak, A. Gagor, D. Stefańska, J. K. Zareba and A. Sieradzki, *Chem. Mater.*, 2020, **32**, 1667–1673.
26 M. Mączka, M. Ptak, D. L. M. Vasconcelos, L. Giriunas, P. T. C. Freire, M. Bertmer, J. Banys and M. Simenas, *J. Phys. Chem. C*, 2020, **124**, 26999–27008.
27 M. Mączka, A. Gagor, J. K. Zareba, D. Stefanska, M. Drozd, S. Balciunas, M. Šimėnas, J. Banys and A. Sieradzki, *Chem. Mater.*, 2020, **32**, 4072–4082.
28 H. Y. Zhang and R. G. Xiong, *Chem. Commun.*, 2022, **59**, 920–923.
29 H. Y. Zhang, X. G. Chen, Z. X. Zhang, X. J. Song, T. Zhang, Q. Pan, Y. Zhang and R. G. Xiong, *Adv. Mater.*, 2020, **32**, 1–8.
30 S. Huang, P. Huang, L. Wang, J. Han, Y. Chen and H. Zhong, *Adv. Mater.*, 2019, **31**, 1903830.
31 A. Sadhanala, F. Deschler, T. H. Thomas, S. E. Dutton, K. C. Goedel, F. C. Hanusch, M. L. Lai, U. Steiner, T. Bein, P. Docampo, D. Cahen and R. H. Friend, *J. Phys. Chem. Lett.*, 2014, **5**, 2501–2505.
32 S. Aharon, B. El Cohen and L. Etgar, *J. Phys. Chem. C*, 2014, **118**, 17160–17165.
33 E. T. Hoke, D. J. Slotcavage, E. R. Dohner, A. R. Bowring, H. I. Karunadasa and M. D. McGehee, *Chem. Sci.*, 2015, **6**, 613–617.
34 G. E. Eperon, S. D. Stranks, C. Menelaou, M. B. Johnston, L. M. Herz and H. J. Snaith, *Energy Environ. Sci.*, 2014, **7**, 982.
35 H. Yu, F. Wang, F. Xie, W. Li, J. Chen and N. Zhao, *Adv. Funct. Mater.*, 2014, **24**, 7102–7108.
36 Y. Nakamura, N. Shibayama, A. Hori, T. Matsushita, H. Segawa and T. Kondo, *Inorg. Chem.*, 2020, **59**, 6709–6716.
37 R. A. Kerner, T. H. Schloemer, P. Schulz, J. J. Berry, J. Schwartz, A. Sellinger and B. P. Rand, *J. Mater. Chem. C*, 2019, **7**, 5251–5259.
38 G. M. Sheldrick, *Acta Crystallogr., Sect. C:Struct. Chem.*, 2015, **71**, 3–8.
39 G. M. Sheldrick, *Acta Crystallogr., Sect. A:Found. Crystallogr.*, 2008, **64**, 112–122.
40 O. V. Dolomanov, L. J. Bourhis, R. J. Gildea, J. A. K. Howard and H. Puschmann, *J. Appl. Crystallogr.*, 2009, **42**, 339–341.